

See discussions, stats, and author profiles for this publication at: <https://www.researchgate.net/publication/228367457>

# Gas– Solid Turbulent Flow in a Circulating Fluidized Bed Riser: Numerical Study of Binary Particle Systems

ARTICLE *in* INDUSTRIAL & ENGINEERING CHEMISTRY RESEARCH · SEPTEMBER 2009

Impact Factor: 2.59 · DOI: 10.1021/ie8015297

---

CITATIONS

23

READS

42

## 5 AUTHORS, INCLUDING:



Niels G Deen

Technische Universiteit Eindhoven

175 PUBLICATIONS 3,006 CITATIONS

[SEE PROFILE](#)



M. Van Sint Annaland

Technische Universiteit Eindhoven

273 PUBLICATIONS 5,713 CITATIONS

[SEE PROFILE](#)



Hans A. M. Kuipers

Technische Universiteit Eindhoven

436 PUBLICATIONS 9,478 CITATIONS

[SEE PROFILE](#)

# Gas–Solid Turbulent Flow in a Circulating Fluidized Bed Riser: Numerical Study of Binary Particle Systems

Y. He,<sup>†,‡</sup> N. G. Deen,<sup>\*,†</sup> M. van Sint Annaland,<sup>†</sup> and J. A. M. Kuipers<sup>†</sup>

Faculty of Science and Technology, Institute of Mechanics Processes and Control Twente (IMPACT), University of Twente, PO Box 217, NL-7500 AE Enschede, The Netherlands, and Department of Power Engineering, College of Energy Science and Engineering, Harbin Institute of Technology, Harbin 150001, China

Numerical simulations were performed of a turbulent gas-particle multiphase flow in a circulating fluidized bed riser using a hard-sphere discrete particle model (DPM) for the particle phase and the Navier–Stokes equations for the gas phase, where the subgrid scale stresses (SGS) were modeled with the SGS model proposed by Vreman.<sup>1</sup> The model enables the simulation of systems with an arbitrary particle size distribution. In this work, binary mixtures of particles with different diameters were studied. From the numerical results it is found that the particles display size distribution in both horizontal and vertical directions. Small particles have a higher vertical particle velocity than the large particles. With increasing superficial gas velocity, the vertical particle velocity is increased. The average particle velocity and concentration vary both in the horizontal and vertical directions. Finally, the numerical results are compared with the experimental and numerical results of Mathiesen et al.<sup>2</sup> It is found that the simulation results with Vreman's SGS model agree better with the literature data than those obtained with a classical Smagorinsky<sup>3</sup> model, especially in the zone close to the wall.

## 1. Introduction

Gas–solid fluidization in circulating fluidized beds are widely encountered in industry such as in coal combustion, catalytic cracking of petroleum, and nuclear industries, etc. A lot of research work has been done to investigate the gas–solid two-phase flow in this apparatus assuming that all particles have identical diameter and density.<sup>4–17</sup> However, in actual circulating fluidized beds often particles with different diameters and different densities are present. The objective of this work is to elucidate the behavior of the different solid phases, which will be helpful to better understand the real flow in circulating fluidized beds and to improve the design and application of the circulating fluidized beds. In a gas–solids riser flow, the hydrodynamic flow characteristics of both gas and solids phases can be strongly heterogeneous, represented by the nonuniform distributions of solids concentration and phase velocities in both the vertical and horizontal directions. The vertical nonuniformity is due to the phase acceleration, whereas the horizontal nonuniformity is mainly caused by the wall boundary effect. The heterogeneous flow structure is still poorly understood, especially for a riser with different solids phases.

Segregation of particles is an important phenomenon in many industries. Particles of different sizes or different densities have different effects on the flow behavior. To shed some light on these effects, most researchers started by investigating binary mixtures. Jenkins and Mancini<sup>18</sup> extended the kinetic theory for granular flow with corrections of the granular temperature for the individual phases. Gidaspow et al.<sup>19</sup> and Manger<sup>20</sup> extended the kinetic theory to binary solids mixtures, applying a separate granular temperature for each particle phase. Applying the latter model, Mathiesen et al.<sup>1,21</sup> studied the particle dynamics of binary mixtures with various sizes in a riser. Huilin and Gidaspow<sup>14</sup> used a similar model to study binary granular

mixtures. Goldschmidt et al.<sup>22</sup> used a multifluid Eulerian model to study the influence of the restitution coefficient on the segregation behavior in dense gas–fluidized bed. In the Lagrangian model, an arbitrary particle size or density distribution can be used, because the physical properties can be defined for each individual particle. Lagrangian models are more straightforward to apply for studying the flow with binary particle mixtures, since it is relatively easy to obtain the behavior of different particle phases and the distribution and segregation of particles. For this reason, this method is becoming more and more popular to simulate the flow behavior in bidisperse gas–solid fluidized beds. Zhou et al.<sup>23</sup> adopted the Lagrangian approach to simulate the gas–particle flow structure in a circulating fluidized bed riser with binary mixtures of particles. Bokkers et al.<sup>24</sup> executed a numerical study on mixing and segregation in a bidisperse gas–solid fluidized bed with a DPM.

In this work, a hard-sphere discrete particle model is used to predict the turbulent flow in a circulating fluidized bed riser. The applied hard-sphere model was first reported by Hoomans et al.<sup>25</sup> In our simulations we applied the SGS model of Vreman<sup>1</sup> to model the subgrid scale stresses, and the simulation results will be compared with those predicted with the standard Smagorinsky<sup>3</sup> model. The Vreman<sup>1</sup> model is constructed in such a way that its dissipation is relatively small in near-wall regions, which implies that application of wall functions is not necessary. It is expected that the better wall treatment would improve the simulation results. Binary mixtures of particles with different diameters are introduced into the bed to investigate the particle behavior as a function of the particle size. Different superficial gas velocities are imposed to investigate the influence on the segregation and the flow statistics. The effect of the particle restitution coefficient on the flow is studied as well. Numerical results of quasi-2D and 3D approaches are compared. Furthermore, the influence of particle size and size distribution on the flow pattern in a circulating fluidized bed riser will be discussed. Finally, the numerical results are compared with experimental and numerical data of Mathiesen et al.<sup>2</sup>

\* To whom correspondence should be addressed. Tel.: +31-53-489 4138. Fax: +31-53-489 2882, E-mail: N.G.Deen@utwente.nl.

<sup>†</sup> University of Twente.

<sup>‡</sup> Harbin Institute of Technology.

## 2. Governing Equations

**2.1. Description of the Gas Phase.** The gas flow is modeled by the volume-averaged Navier–Stokes equations:

$$\frac{\partial(\varepsilon_g \rho_g)}{\partial t} + \nabla(\varepsilon_g \rho_g \mathbf{u}_g) = 0 \quad (1)$$

$$\frac{\partial(\varepsilon_g \rho_g \mathbf{u}_g)}{\partial t} + \nabla(\varepsilon_g \rho_g \mathbf{u}_g \mathbf{u}_g) = -\varepsilon_g \nabla P - \mathbf{S}_p - \nabla(\varepsilon_g \tau_g) + \varepsilon_g \rho_g \mathbf{g} \quad (2)$$

Here,  $\varepsilon_g$  is the porosity, and  $\rho_g$ ,  $\mathbf{u}_g$ ,  $\tau_g$ , and  $P$ , respectively, are the density, velocity, viscous stress tensor, and pressure of the gas phase, respectively. The source term  $\mathbf{S}_p$  is defined as:

$$\mathbf{S}_p = \frac{1}{V} \int \sum_{a=0}^{N_{\text{part}}} \frac{\beta V_a}{1 - \varepsilon_g} (\mathbf{u}_g - \mathbf{v}_a) \delta(\mathbf{r} - \mathbf{r}_a) dV \quad (3)$$

Here  $V$  is the volume of the fluid cell,  $V_a$  the particle volume,  $\mathbf{v}_a$  the particle velocity, and  $N_{\text{part}}$  the number of particles. The distribution-function  $\delta$  distributes the reaction force of the particles exerted on the gas phase to the velocity nodes on the (staggered) Eulerian grid. To calculate the interphase momentum exchange coefficient  $\beta$  we employed the well-known Ergun<sup>26</sup> equation for porosities lower than 0.8 and the Wen and Yu<sup>27</sup> correlation for porosities higher than 0.8.<sup>28</sup>

$$\beta = \begin{cases} 150 \frac{\mu_g \varepsilon_s^2}{\varepsilon_g^2 d_p^2} + 1.75 \frac{\rho_g \varepsilon_s}{\varepsilon_g d_p} |\mathbf{u}_g - \mathbf{v}_a| & \forall \varepsilon_g \leq 0.8 \\ \frac{3C_d \varepsilon_s \varepsilon_g \rho_g |\mathbf{u}_g - \mathbf{v}_a|}{4d_p} \varepsilon_g^{-2.65} & \forall \varepsilon_g > 0.8 \end{cases} \quad (4)$$

with

$$Re_p = \frac{\rho_g |\mathbf{u}_g - \mathbf{v}_a| d_p}{\mu_g} \quad (5)$$

$$C_d = \begin{cases} \frac{24}{Re_p} (1 + 1.15 Re_p^{0.687}) & \forall Re_p < 1000 \\ 0.44 & \forall Re_p \geq 1000 \end{cases} \quad (6)$$

where  $Re_p$ ,  $d_p$ , and  $\mathbf{v}_a$  are respectively the particle Reynolds number, diameter, and velocity.  $\varepsilon_s$  and  $C_d$  are the local solids volume fraction and the drag coefficient, respectively. It is known that this drag relation has a discontinuity around the switching value of  $\varepsilon_g = 0.8$ . However, since the local instantaneous particle volume fraction is generally below  $\varepsilon_s = 0.2$ , this has no effect on the simulation results in this work.

The gas-phase stress tensor in eq 2 is given by:

$$\tau_g = -\mu_{g,\text{eff}} ((\nabla \mathbf{u}_g) + (\nabla \mathbf{u}_g)^T - \frac{2}{3} \mathbf{I} (\nabla \mathbf{u}_g)) \quad (7)$$

We do not resolve all the details of the flow as one would do in a DNS. Hence, a SGS model is required to account for the unresolved subgrid scale stresses, which are included through the eddy viscosity  $\mu_{g,\text{eff}}$ . Since the DPM is a full 3D, time-resolved model, the choice for a SGS model is much more natural than a RANS type of model, such as the  $k-\varepsilon$  model, which is based on averaging the equations.

The eddy viscosity of the gas is calculated by the SGS model of Vreman:<sup>1</sup>

$$\mu_{g,\text{eff}} = c \rho \sqrt{\frac{B_\beta}{\alpha_{ij} \alpha_{ij}}} \quad (8)$$

with

$$\alpha_{ij} = \frac{\partial u_{g,j}}{\partial x_i} \quad (9)$$

$$\beta_{ij} = \Delta_m^2 \alpha_{mi} \alpha_{mj} \quad (10)$$

$$B_\beta = \beta_{11} \beta_{22} - \beta_{12}^2 + \beta_{11} \beta_{33} - \beta_{13}^2 + \beta_{22} \beta_{33} - \beta_{23}^2 \quad (11)$$

Here  $c$  and  $\Delta_m$  are respectively a model constant and the local filter width, which will be explained later. Note that the index  $m$  in eq 10 indicates a summation over all three coordinate directions. The symbol  $\alpha$  stands for the  $(3 \times 3)$  matrix of derivatives of the filtered velocity  $\mathbf{u}_g$ . We define that if  $\|\alpha_{ij} \alpha_{ij}\| = 0$ , then  $\mu_{g,\text{eff}} = 0$  (where  $\|\cdot\|$  is the norm).

The Smagorinsky<sup>3</sup> model is given by:

$$\mu_{g,\text{eff}} = \rho (C_s \Delta)^2 \|S_{ij} S_{ij}\| \quad (12)$$

where  $S_{ij} = (1/2)(\partial \mathbf{u}/\partial x_i) + (1/2)(\partial \mathbf{u}/\partial x_j)$  is the characteristic filtered strain rate. The model constant  $c$  is related to the Smagorinsky constant  $C_s$  by  $c \approx 2.5 C_s^2$ . In our simulation we let  $C_s = 0.1$  (i.e.,  $c = 0.025$ ). Both turbulence models can be implemented in the DPM straightforwardly, since it only requires the local filter width and the first-order derivatives of the velocity field. The gas-phase equations are solved numerically with a finite differencing technique, in which a staggered grid was

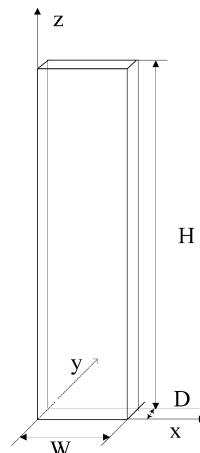


**Figure 1.** Schematic representation of the fluidized bed riser.

**Table 1. Parameters Used in the Base Case<sup>a</sup>**

parameter	value
particle diameter, $d_p$	120 and 185 ( $\mu\text{m}$ )
overall volume fraction for each class, $\varepsilon_s$	1.25% and 1.25% (-)
particle density, $\rho_p$	2400 ( $\text{kg}/\text{m}^3$ )
normal restitution coefficient, $e_n$	0.97 (-)
tangential restitution coefficient, $\beta_0$	0.33 (-)
friction coefficient, $\mu$	0.10 (-)
CFD time step	$5.0 \times 10^{-5}$
particle time step, $\Delta t$	$5.0 \times 10^{-5}$
channel width, $W$	0.032 (m)
channel depth, $D$	0.0012 (m)
channel height, $H$	0.30 (m)
CFD grid number, $N_x$	25 (-)
CFD grid number, $N_y$	1 (6) (-)
CFD grid number, $N_z$	60 (-)
shear viscosity of gas, $\mu_g$	$1.8 \times 10^{-5}$ (Pa·s)
gas temp, $T$	313 (K)
pressure, $P$	1.2 (Bar)
velocity, $u_g$	1.0 (1.2) (m/s)
particle terminal velocities (120 and 185 $\mu\text{m}$ ), $u_t$	0.92 and 1.42 (m/s)
number of particles, $N_p$	20260 (-)

<sup>a</sup> Values used in alternative cases are indicated in parentheses.

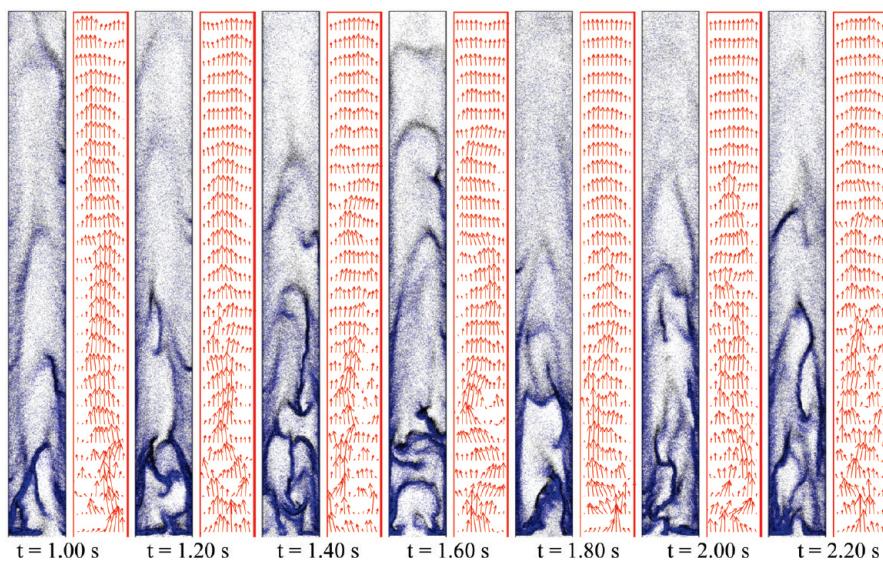


**Figure 2.** Time series of the gas-particle flow and velocity of gas phase in the riser.

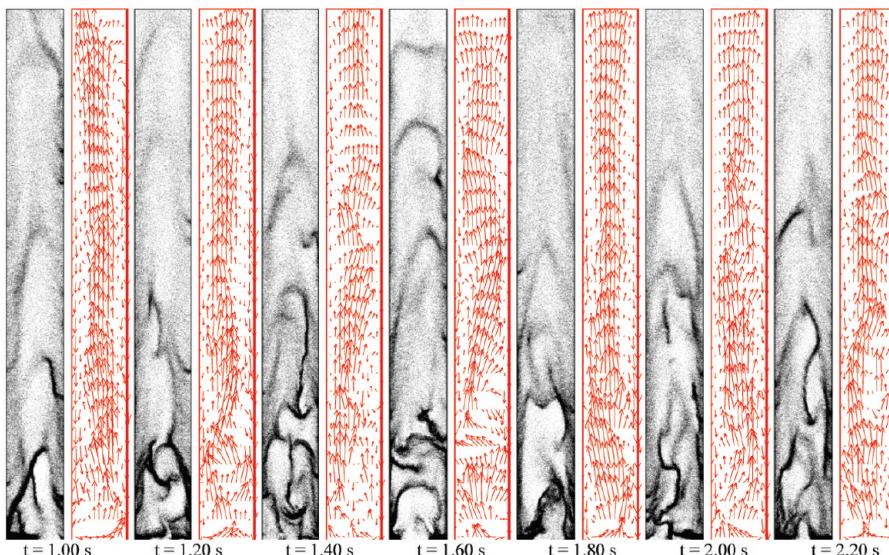


**Figure 3.** Time series of the gas-particle flow and the velocity of particles in the riser for small particles ( $d_p = 120 \mu\text{m}$ ).

employed to ensure numerical stability. In this work the effect of the SGS turbulent structures on the particle dynamics can be safely ignored, owing to the high particle Stokes numbers. The effect of the particles on the turbulence on the other hand is not very well understood and is therefore as a first approximation ignored in this work.

**2.2. Description of the Solid Phase.** The hard-sphere discrete particle model (DPM) used in this work was originally developed by Hoomans et al.<sup>25</sup> In the DPM the particles are assumed to be rigid spheres moving in free flight. When collisions among particles occur, these are treated as binary, instantaneous, impulsive events.

The velocity of every individual particle can be calculated from Newton's second law, containing forces due to the pressure gradient, drag, and gravitation:

$$m_a \frac{d^2 \mathbf{r}_a}{dt^2} = \frac{V_a \beta}{1 - \varepsilon} (\mathbf{u}_g - \mathbf{v}_a) - V_a \nabla P + m_a \mathbf{g} \quad (13)$$

$$I_a \Omega_a = I_a \frac{d\omega_a}{dt} = \mathbf{T}_a \quad (14)$$

Here,  $m_a$  is the mass of the particle,  $\mathbf{T}_a$  the torque,  $I_a$  the moment

of inertia,  $\Omega_a$  the rotational acceleration, and  $\omega_a$  the rotational velocity.

In this model, it is assumed that the interaction forces are impulsive and therefore all other finite forces are negligible during collisions. Consider two colliding spheres  $a$  and  $b$  with position vectors  $\mathbf{r}_a$  and  $\mathbf{r}_b$ . The particle velocities prior-to-collision are indicated by the subscript 0 and the relative velocity at the contact point  $c$  is defined as:

$$\mathbf{v}_{ab} \equiv \mathbf{v}_{a,c} - \mathbf{v}_{b,c} \quad (15)$$

For a binary collision of these spheres the following equations can be derived by applying Newton's second and third law.

$$\mathbf{J} = m_{p,a}(\mathbf{v}_a - \mathbf{v}_{a,0}) = -m_{p,b}(\mathbf{v}_b - \mathbf{v}_{b,0}) \quad (16)$$

$$-\mathbf{n} \times \mathbf{J} = \frac{I_a}{R_a}(\omega_a - \omega_{a,0}) = \frac{I_b}{R_b}(\omega_b - \omega_{b,0}) \quad (17)$$

where the moment of inertia is given by:

$$I = \frac{2}{5}mR^2 \quad (18)$$

and the normal vector is given by:

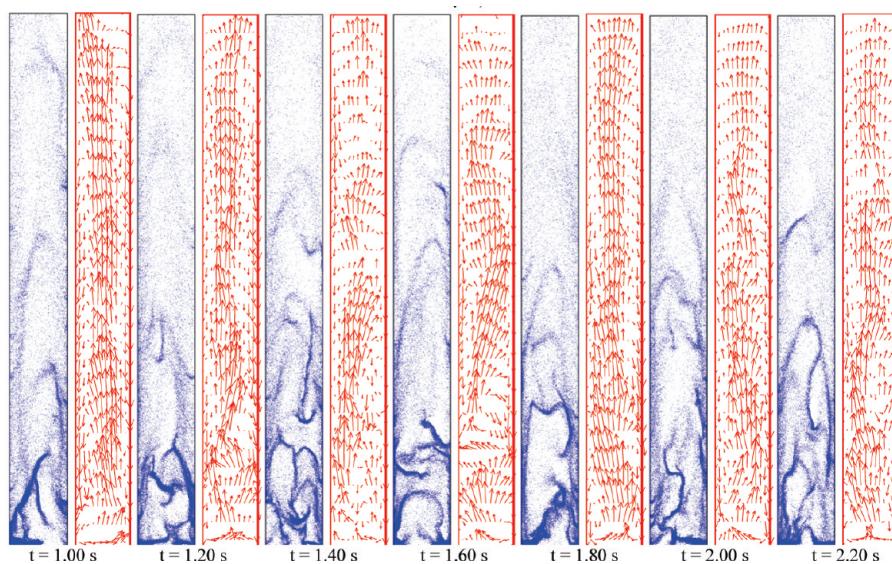


**Figure 4.** Time series of the gas-particle flow and the velocity of particles in the riser for large particles ( $d_p = 185 \mu\text{m}$ ).

$$\mathbf{n} = \frac{\mathbf{r}_a - \mathbf{r}_b}{|\mathbf{r}_a - \mathbf{r}_b|} \quad (19)$$

Equations 15 and 16 can be rearranged to obtain:

$$\mathbf{v}_{ab} - \mathbf{v}_{ab,0} = \frac{7\mathbf{J} - 5\mathbf{n}(\mathbf{J} \cdot \mathbf{n})}{2m_{ab}} \quad (20)$$

where the reduced mass  $m_{ab}$  is given by:

$$m_{ab} = \left( \frac{1}{m_a} + \frac{1}{m_b} \right)^{-1} \quad (21)$$

In order to calculate the postcollision velocities, a closure model consisting of three parameters is used to describe the momentum vector  $\mathbf{J}$ . The first parameter is the coefficient of normal restitution:

$$\mathbf{v}_{ab} \cdot \mathbf{n} = -e_n(\mathbf{v}_{ab,0} \cdot \mathbf{n}) \quad (22)$$

Here  $e_n$  is the normal restitution coefficient. The second parameter is the coefficient of dynamic friction:

$$|\mathbf{J} \times \mathbf{n}| = -\mu(\mathbf{J} \cdot \mathbf{n}) \quad (23)$$

Here  $\mu$  is the friction coefficient. The third parameter is the coefficient of the tangential restitution:

$$\mathbf{v}_{ab} \cdot \mathbf{t} = -\beta_0(\mathbf{v}_{ab,0} \cdot \mathbf{t}) \quad (24)$$

where  $\beta_0$  is the tangential restitution coefficient.

Combining eqs 22 and 23 yields the following expression for the normal component of the momentum vector:

$$J_n = -(1 + e_n)m_{ab}\mathbf{v}_{ab,0} \cdot \mathbf{n} \quad (25)$$

For the tangential component, two types of collisions can be distinguished, i.e. sticking and sliding collisions. If the tangential component of the relative velocity is sufficiently high in comparison to the coefficient of friction and tangential restitution, gross sliding occurs throughout the whole duration of the contact and the collision is of the sliding type. The nonsliding collisions are of the sticking type. When  $\beta_0$  is equal to zero, the tangential component of the relative velocity becomes zero during a sticking collision. When  $\beta_0$  is greater than zero in such a collision, reversal of the tangential component of the relative velocity will occur. The criterion to determine the type of collision on basis of precollision is as follows:

$$J_t = \begin{cases} -\frac{2}{7}(1 + \beta_0)\mathbf{v}_{ab,0} \cdot \mathbf{t} & \text{if } \mu J_n < \frac{2}{7}(1 + \beta_0)m_{ab}\mathbf{v}_{ab,0} \cdot \mathbf{t} \\ -\mu J_n & \text{otherwise} \end{cases} \quad (26)$$

where the two equations respectively describe collisions of the sticking and sliding type. Given the definition of  $\mathbf{J}$  in eqs 25 and 26, the postcollision velocities can now be calculated from eqs 22 and 24. In particle-wall collisions the mass of particle  $b$  (i.e., the wall) is taken infinitely large, which makes all terms  $1/m_b$  equal to zero. The particle collision characteristics play an important role in the overall system behavior, as was shown by Hoomans et al.<sup>25</sup> and Goldschmidt et al.<sup>22</sup> For this reason realistic collision properties of the particles are supplied to the model, i.e. the coefficients of the normal and tangential restitution are respectively set to  $e_n = 0.97$  and  $\beta_0 = 0.33$ , and the coefficient of friction is set to  $\mu = 0.1$ . The restitution and friction coefficients are assumed to be independent of the relative velocity and collision angle. Note that the same collision properties are used for collisions between particles and the confining walls.

### 3. Initial and Boundary Conditions

A sketch of the fluidized bed riser simulated in this study is shown in Figure 1. The simulations are carried out only for the central part of the riser without considering the inlet and exit effects. Initially, the particles are distributed evenly across the flow domain to achieve a uniform initial concentration distribution. Each particle that crosses one of the top or bottom boundaries is inserted again at the opposite boundary while retaining all of its physical properties. The use of these boundary conditions implies that the total number of particles in the flow domain, i.e. the overall particle volume fraction, remains constant. Gas is injected at a constant uniform flow rate at the bottom of the column, and a pressure boundary condition is used for the gas phase at the top of the bed. No-slip conditions are used for the gas phase at the left and right walls, while free slip boundary conditions are applied at the front and back wall. The physical parameters are chosen in accordance with the work of Mathiesen et al.,<sup>2</sup> who carried out a combined experimental and numerical study of the flow in a riser. In our work, the channel height is less than that in the case of Mathiesen et al.,<sup>2</sup> so the number of the particles was reduced to match the overall

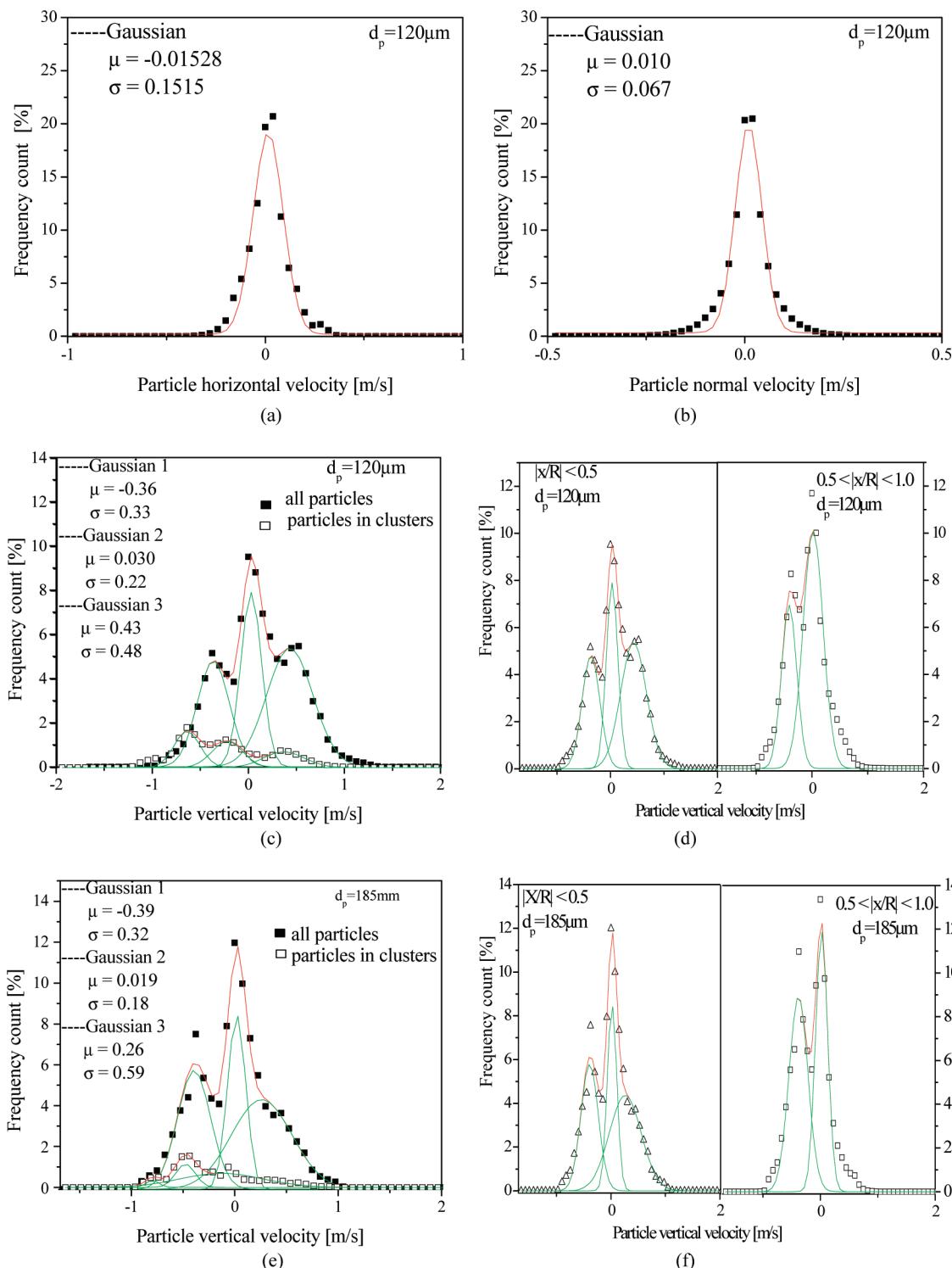


**Figure 5.** Particle velocity distributions for small particles and large particles at  $t = 8.00$  s.

particle volume fraction. The simulation parameters for the base case are listed in Table 1, along with two alternative cases, i.e. with a different superficial gas velocity and a different computational grid. The average volume fraction for the small and large particles is equal. All simulations were run for 8 s, and time averages were calculated during the last 5 s. Although this averaging period is relatively short, it is sufficiently long to illustrate the trends in the fluidization dynamics. It is noted that, to obtain fully converged simulation results, unpractical simulation times of several months would be required.

The applied numerical grid was selected in such way that all relevant structures are resolved, while ensuring that the particle

volumes are significantly smaller than the volume of a grid cell. The simulations presented in this work have a degree of accuracy similar to that in the work of Vreman et al.,<sup>29</sup> who uses similar simulation conditions and who has argued that the grid is sufficiently fine. This implies that a (very costly) grid sensitivity study is not necessary.

#### 4. Simulation Results

In this section the simulation results are presented. First, we will discuss the overall flow patterns. Subsequently, we will discuss the particle velocity distribution, followed by a

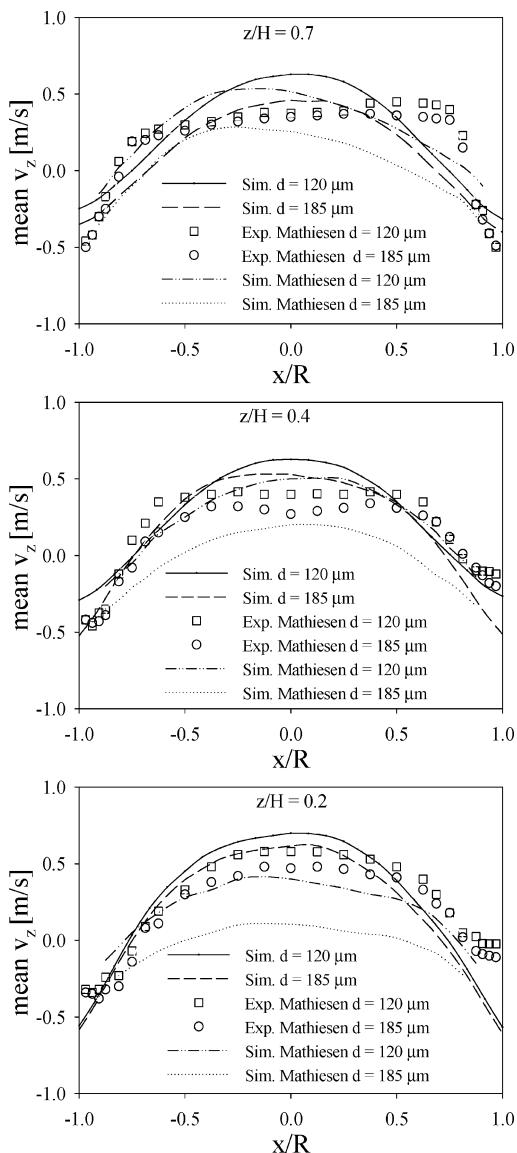


**Figure 6.** Particle vertical velocity profiles at different heights.

detailed comparison with experimental and numerical data from the literature for two different superficial velocities. Finally, we will discuss the effect of the collisional properties, the turbulence model, and the choices made for the computational geometry.

**4.1. Overall Flow Patterns.** Figure 2 shows a time series of the computed flow patterns and the velocities of the gas phase in the riser. The particles form horseshoe shaped clusters that move both in upward and downward directions. The clusters form, grow, change their shape and finally break up. After breaking up, the particles are collected near the walls. The particles tend to concentrate near the bottom of the bed. The velocities of the gas phase are all positive, showing the largest values in the core of the bed. The gas velocity is considerably reduced in the vicinity of the clusters.

Figures 3 and 4 show time series of the particle distribution and the velocity of the small particles and large particles, respectively. Particles are moving upward in the bed center and flow downward close to the walls. From these figures, the status of clusters can be clearly observed. Particles that are inside a cluster flow with low velocities. A typical core-annulus flow pattern is observed in the snapshots. The flow patterns for the particles of the two size classes are nearly the same, while the

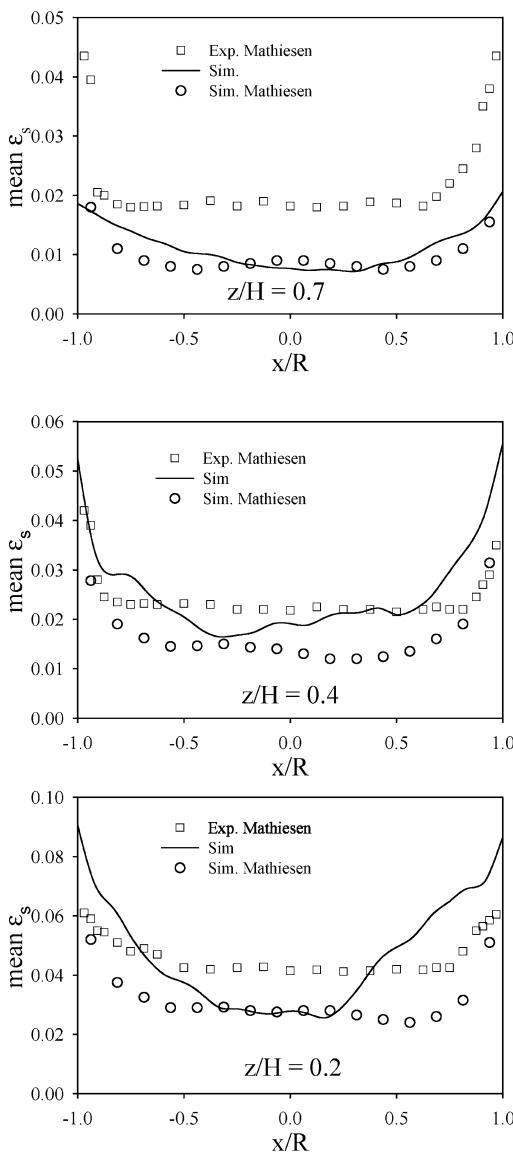


**Figure 7.** Mean volume fraction profiles of particles at different heights.

velocity and volume fraction of particles differ, indicating significant particle segregation.

**4.2. Particle Velocity Distribution.** Figures 5a to 5d and 5e to 5f show the velocity distributions of the small and the large particles, respectively, at  $t = 8.0$  s. The horizontal ( $v_{p,y}$ ) and normal ( $v_{p,x}$ ) velocity distributions for small particles are approximately Gaussian, which is illustrated in Figures 5a and 5b, respectively. Figures 5c and 5d show the vertical velocity distribution for small particles in the entire bed and in various regions, respectively. The vertical ( $v_{p,z}$ ) velocity distribution of all particles in the riser contains three distinct peaks, each of which is fitted with a Gaussian distribution. Each peak reflects a different type of particle flow behavior, i.e. up and downward moving clusters and upward moving isolated particles. The velocity distribution is different in the core and the annulus of the riser. As can be observed from Figure 5d, the velocity distribution in center of the riser is similar to that in the entire system. However, it is totally different in the region close to the wall, where two clear peaks appear. This is related to the fact that in the annulus, clusters are predominantly moving downward. Figures 5e and 5f show the vertical velocity distribution of large particles in the entire bed and in two different regions of the bed, respectively. Compared with

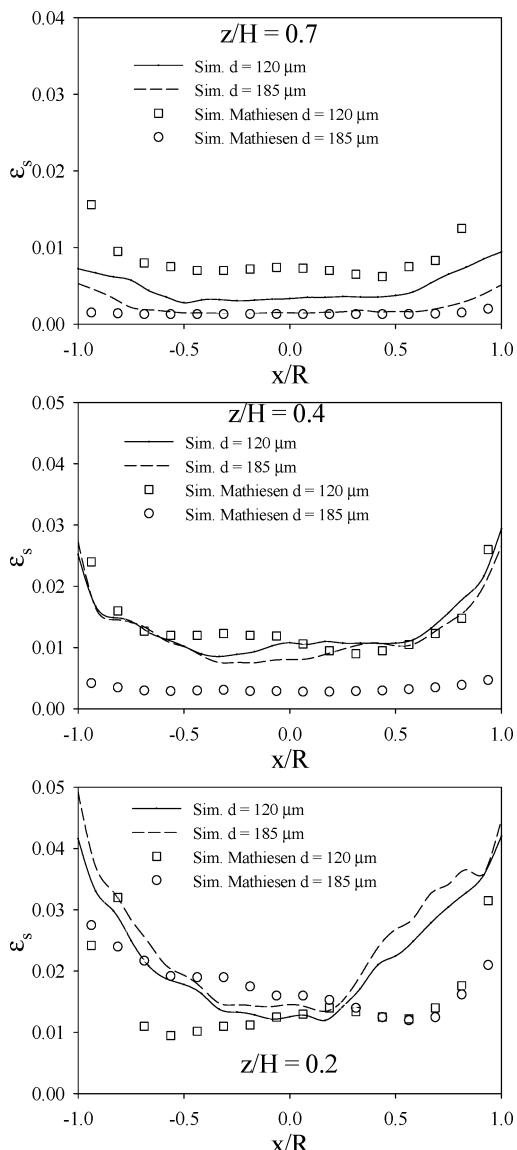


**Figure 8.** Volume fraction profiles of small particles and large particles at different heights.

the distribution of small particles, it is observed that the third peak is less distinct. Similar to the small particles, the large particles display three peaks in the center of the bed and two peaks in the near-wall region. The observed trends in the variance between the large particles and the small particles imply that the anisotropic character of the particles in a turbulent system becomes more significant with increasing particle size. In the following part of the paper, we will discuss some aspects of the nonlinear character of the system in order to understand this anisotropy more clearly.

**4.3. Quantitative Comparison of Particle Dynamics.** Figure 6 shows the average vertical particle velocity at different heights. A typical core-annulus flow structure is observed, that is to say that upflow takes place in the center of the riser, while sharp velocity gradients and particle downflow are found near the walls. The latter can be related to the passage of clusters, which are mostly found near the walls. The asymmetry in the experimental data is probably related to inlet effects. The simulated results agree well with the experimental and numerical results of Mathiesen et al.<sup>2</sup> Our simulation results agree somewhat better with the experimental results than the computational result of Mathiesen et al.<sup>2</sup> especially in the zone near

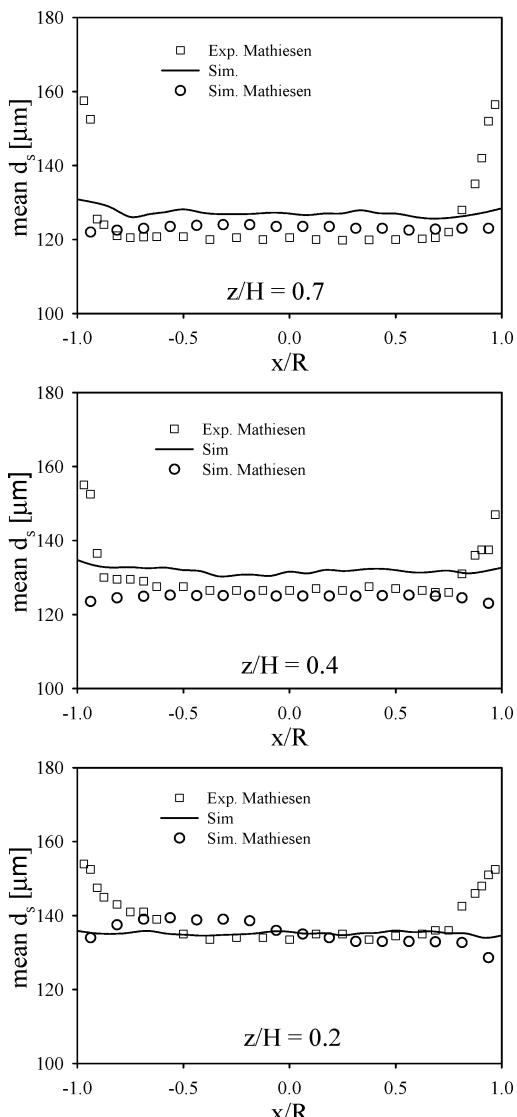


**Figure 9.** Mean diameter profiles of particles at different heights.

the bottom of the bed when  $z/H = 0.2$ . It is seen that the DPM is better able to predict the small velocity differences between the particles than the multifluid model of Mathiesen et al.<sup>2</sup>

Figure 7 shows volume fraction profiles of particles at different heights in the riser. The concentration of particles is low in the bed center and high near the walls where clusters are mostly found. The particle volume fraction decreases with increase in bed height. The numerical result is compared with the experimental and numerical results of Mathiesen et al.<sup>2</sup> All results show the same tendencies.

Figure 8 shows the volume fraction profiles of both particle size classes at different heights in the riser. The volume fractions of both small and large particles are high close to the walls and decrease along the horizontal direction. There are less large than small particles in the upper part of the bed. In the lower part of the bed the opposite trend is observed. In the middle of the bed the simulation result shows that the volume fractions of both particle phases are approximately the same. The numerical results are compared with the computational results of Mathiesen et al.,<sup>2</sup> who reported the same tendencies.

Profiles of the mean particle diameter at different heights are presented in Figure 9. The mean diameter has the same tendency as the results of Mathiesen et al.<sup>2</sup> Generally speaking, the mean diameter is larger near the walls than in the bed center and larger

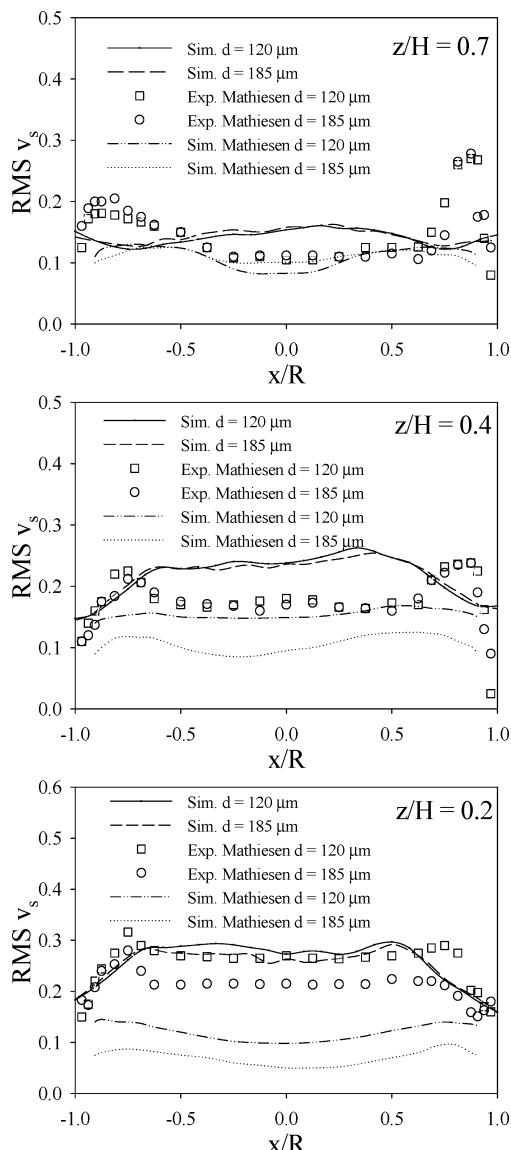


**Figure 10.** Particle fluctuating velocity distributions at different heights.

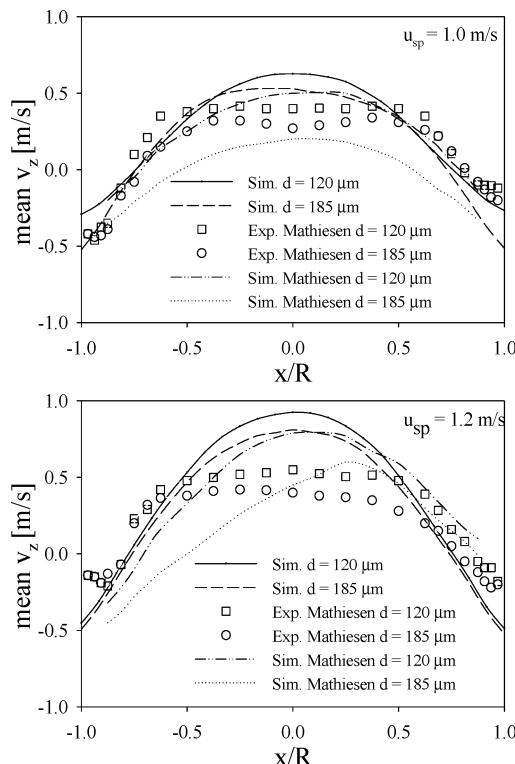
in the bottom zone of the bed than in the upper zone of the bed. The mean diameter agrees well with the experimental results at the bottom of the bed. However, our numerical results in the upper part of the bed are a bit overpredicted.

Figure 10 shows the rms velocity distribution of both phases at different heights. For the convenience of comparison, we define the rms velocity of the particle phase in the same way as Mathiesen et al.<sup>2</sup>

$$V_{\text{rms}} = \sqrt{3\theta_s} \quad (27)$$

where  $\theta_s$  is the granular temperature. At all heights the rms velocities of particles of both sizes are low at the wall, then increase to a local maximum near the wall, and subsequently decrease along the horizontal direction. The rms velocities of particles of both sizes are nearly the same in the upper and middle parts of the bed. Small particles have larger rms velocities in the bottom part of the bed. Our numerical results agree better with the experimental results than the numerical results of Mathiesen et al.<sup>2</sup> especially in the bottom part of the bed.

**4.4. Superficial Velocity.** Superficial gas velocities of 1.0 and 1.2 m/s are used in the simulations to study the influence



**Figure 11.** Particle velocity profiles at different superficial gas velocities,  $z/H = 0.4$ .

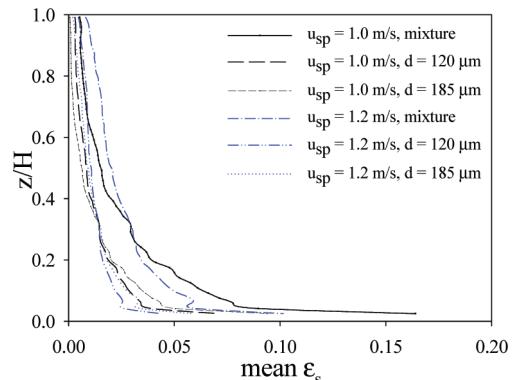


**Figure 12.** Computational particle volume fractions at different superficial gas velocities.

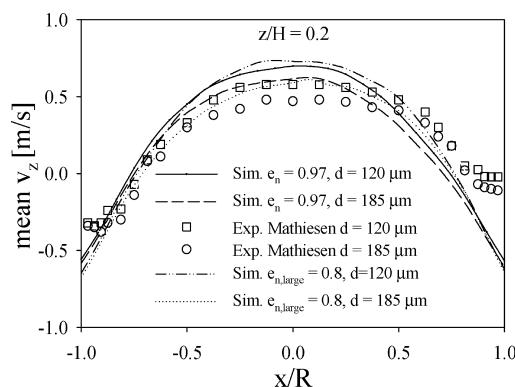


**Figure 13.** Computational particle vertical velocities; effect of collisional properties.

on the flow behavior. Figure 11 gives the particle velocity profiles at different superficial gas velocities at a height of 0.4 m. As expected, the mean velocity of the particles of both sizes

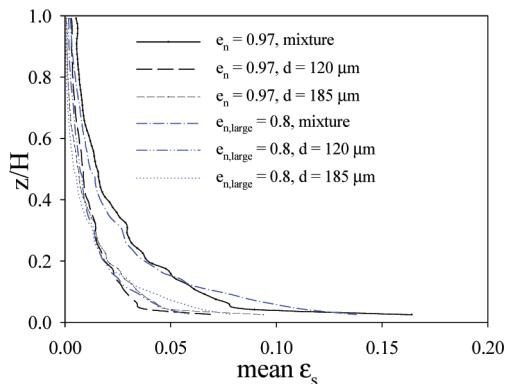


**Figure 14.** Computational particle volume fractions; effect of collisional properties.

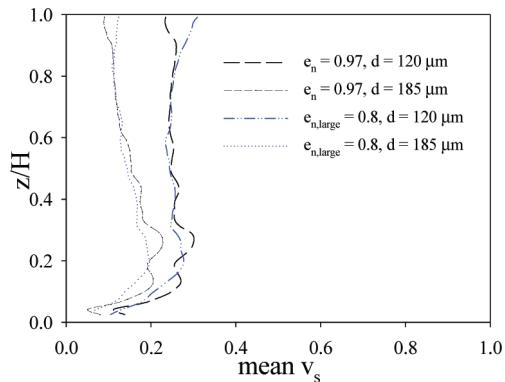


**Figure 15.** Computational particle vertical velocities; effect of collisional properties.

increases with increasing superficial gas velocity. The numerical results agree well with the experimental data near the walls, while the velocities are somewhat overpredicted in the bed center.

Figure 12 shows the computed particle volume fractions at both superficial gas velocities. The particle volume fractions decrease with increasing bed height for each of the particle phases. Comparing the results of both superficial gas velocities, we find that the particles are much better distributed along the bed height when the superficial gas velocity is increased.

**4.5. Influence of Collisional Properties.** As mentioned earlier the particle dynamics are influenced by the collisions of particles. Two simulations with different restitution coefficients (that is  $e_n = 0.97$  for both particle phases, as well as  $e_n = 0.97$  and  $e_n = 0.80$  for the small and the large particles, respectively) were performed to investigate the influence of the collision parameters. Figure 13 shows the mean vertical velocity profile of particles at a height of  $z/H = 0.2$ . We find that the vertical velocity in the bed center is similar to that found in the base case. Figures 14 and 15 give the variation of mean concentration and vertical velocity of particles along the height of the riser. Both profiles change only marginally. Hence, we conclude that, although ideal and nonideal particles are known to behave very differently, the degree of nonideality is less important for large particles in riser flows.

**4.6. Turbulence Model.** In the base case Vreman's SGS model<sup>1</sup> was adopted. In order to compare with the well-known Smagorinsky<sup>3</sup> SGS model, we also executed a simulation with the Smagorinsky SGS model, which now will be discussed. In Figure 16, we can find the velocities profiles at different heights with both SGS models. In general, the results of both SGS models fit equally well with the experimental data in the bed

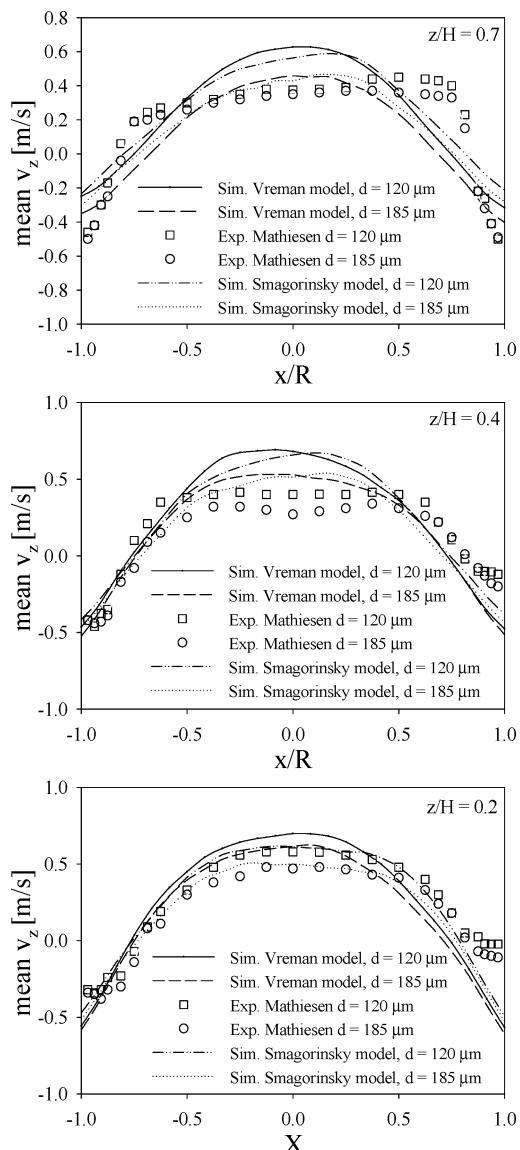


**Figure 16.** Particle velocity profiles at different heights; effect of turbulence model.

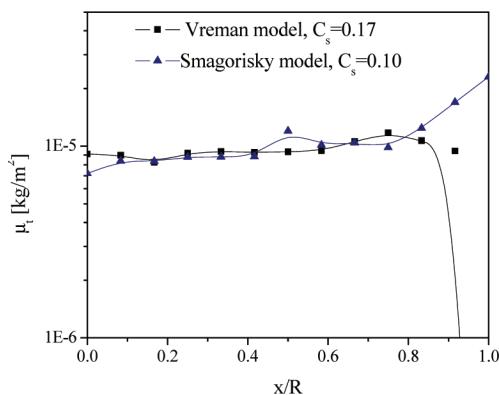


**Figure 17.** Turbulent viscosity variations with horizontal direction at  $z/H = 0.4$ .

center. However, the velocities of the particle phase near the wall show a slightly larger discrepancy when the Smagorinsky model is used. This is attributed to the numerical result for the turbulent viscosity, which is known to be overpredicted by the Smagorinsky SGS model, whereas the SGS model of Vreman<sup>1</sup> was specifically designed to give better results in near wall

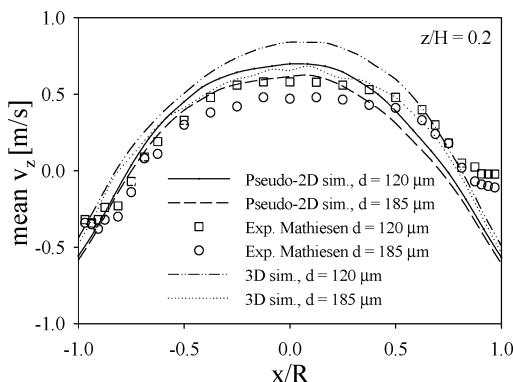


**Figure 18.** Particle velocity profiles; effect of geometry.

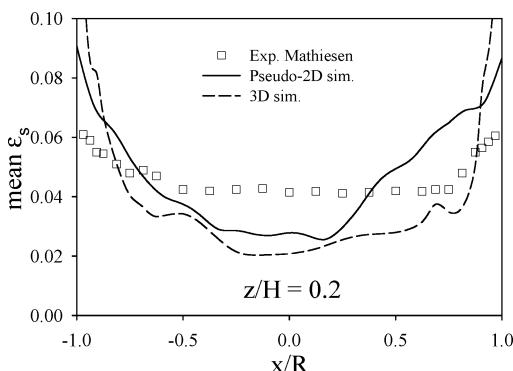


**Figure 19.** Particle concentration profiles; effect of geometry.

regions. The turbulent viscosities of both SGS models are presented in Figure 17.

**4.7. Choice of Geometry.** We adopted a quasi-2D model with only one grid cell in the depth direction of the riser in the base case for the simulation. Because the flow in reality is three-dimensional, a simulation with six grid cells in the depth direction was adopted to compare with the result of a quasi-2D model.

Figures 18 and 19 show the mean particle velocity distribution and mean solid concentration distribution with the quasi-2D model and 3D model, respectively. The results from the 3D model are similar to the results obtained from the quasi-2D model. Thus, it is permissible to use a quasi-2D model, which is favorable because of its lower computational requirements.

## 5. Conclusions

In this paper, we studied the turbulent gas-particle two-phase flow in a circulating fluidized bed riser based on a quasi-2D DPM model. Because both the interparticle collisions and the gas-phase turbulence play important roles in these type of flows, we accounted for these effects in our simulations with the use of a large eddy simulation (LES) turbulence closure proposed by Vreman<sup>1</sup> and four-way coupling.

The following main conclusions were obtained from the work presented in this paper:

(1) The different particle phases show distinctively different behavior. That is to say that small particles experience a larger drag and thus obtain a higher vertical velocity and a more homogeneous vertical distribution.

(2) The turbulent flow in the circulating fluidized bed riser is a typical nonlinear system, which is characterized by three different types of flow behavior, i.e. up and downward moving

clusters and upward moving isolated particles. Near the wall clusters are predominantly moving downward.

(3) Increasing the superficial gas velocity changes the flow behavior in the riser, especially the segregation of the particles.

(4) The particle restitution coefficient has a small influence on the horizontal character and vertical character of the flow.

(5) The SGS model of Vreman<sup>1</sup> is easy to apply in the simulation and is to be preferred over the traditional Smagorinsky<sup>3</sup> model because of its better numerical result near the wall.

(6) 3D numerical results are similar to the quasi-2D numerical results. Hence, a quasi-2D description of the gas phase suffices to describe riser flow.

This work is one of the very first papers to describe riser flow of binary mixtures adopting a DPM model. This study is just a first step to describe processes in a riser. Extension of the model with other particle properties, such as particle temperature and chemical species concentration, is much easier to accomplish than with a multifluid model.

## Acknowledgment

This work was supported by the National Science Foundation through Grant No. 50376013 and NSFC-PetroChina Company Limited under the cooperative project No. 20490200.

## Literature Cited

- Vreman, A. W. An Eddy-viscosity Subgrid-scale Model for Turbulent Shear Flow: Algebraic Theory and Applications. *Phys. Fluids* **2004**, *16*, 3670.
- Mathiesen, V.; Solberg, T.; Hjertager, B. H. An experimental and computational study of multiphase flow behavior in a circulating fluidized bed. *Int. J. Multiphase Flow* **2000**, *26*, 387.
- Smagorinsky, J. General circulation experiments with the primitive equations. *Monthly Weather Rev.* **1963**, *91*, 99.
- Sinclair, J. L.; Jackson, R. Gas-particle flow in a vertical pipe with particle-particle interactions. *AICHE J.* **1989**, *35*, 1473.
- Pita, J. A.; Sundaresan, S. Developing flow of a gas-particle mixture in a vertical riser. *AICHE J.* **1993**, *39*, 541.
- Nieuwland, J. J.; Van Sint Annaland, M.; Kuipers, J. A. M.; Van Swaaij, W. P. M. Hydrodynamic modeling of gas-particle flows in riser reactors. *AICHE J.* **1996**, *42*, 1569.
- Hrenya, C. M.; Sinclair, J. L. Effects of particle-particle turbulence in gas-solids flows. *AICHE J.* **1997**, *43*, 853.
- Samuelsberg, A.; Hjertager, B. H. Computational modeling of gas-particle flow in a riser. *AICHE J.* **1996**, *42*, 1536.
- Benyahia, S.; Arastoopour, H.; Knowlton, T. M.; Massah, H. Simulation of particles and gas flow behavior in the riser section of a circulating fluidized bed using the kinetic theory approach for the particulate phase. *Powder Technol.* **2000**, *112*, 24.
- Dasgupta, S.; Jackson, R.; Sundaresan, S. Gas-particle flow in vertical pipes with high mass loading of particles. *Powder Technol.* **1998**, *96*, 6.
- Neri, A.; Gidaspow, D. Riser hydrodynamics: simulation using kinetic theory. *AICHE J.* **2000**, *46*, 52.
- Helland, E.; Occelli, R.; Tadrist, L. Numerical study of cluster formation in a gas-particle circulating fluidized bed. *Powder Technol.* **2000**, *110*, 210.
- Yamamoto, Y.; Potthoff, M.; Tanaka, T.; Kajishima, T.; Tsuji, Y. Large eddy simulation of turbulent gas-particle flow in a vertical channel: effect of considering inter-particle collisions. *J. Fluid Mech.* **2001**, *442*, 303.
- Hulin, L.; Gidaspow, D. Hydrodynamics of binary fluidization in a riser: CFD simulation using two granular temperatures. *Chem. Eng. Sci.* **2003**, *58*, 3777.
- Wang, S.; Liu, H.; Lu, H.; Liu, W.; Jiamin, D.; Li, W. Flow behavior of clusters in a riser simulated by direct simulation Monte Carlo method. *Chem. Eng. J.* **2005**, *106*, 197.
- Zhao, Y.; Lu, H.; He, Y.; Jianmin, D.; Yin, L. Numerical prediction of combustion of carbon particle clusters in a circulating fluidized bed riser. *Chem. Eng. J.* **2006**, *118*, 1.
- Qi, X. B.; Huang, W. X.; Zhu, J. Comparative Study of Flow Structure in Circulating Fluidized Bed Risers with FCC and Sand Particles. *Chem. Eng. Technol.* **2008**, *31*, 542.

- (18) Jenkins, J. T.; Mancini, F. Kinetic theory for binary mixtures of smooth, nearly elastic spheres. *Phys. Fluids* **1989**, *31*, 2050.
- (19) Gidaspow, D.; Huilin, L.; Manger, E. Kinetic theory of multiphase flow and fluidization: validation and extension to binaries. Proceedings of the XIX<sup>th</sup> International Congress on Theoretical and Applied Mechanics, Kyoto, Japan, Aug 25–31; Elsevier: Amsterdam, 1996.
- (20) Manger, E. Modelling and simulation of gas/solid flow in curvilinear coordinates. Ph.D. thesis, Telemark Institute of Technology, Norway, 1996.
- (21) Mathiesen, V.; Solberg, T.; Arastoopour, H.; Hjertager, B. H. Experimental and computational study of multiphase gas/particle flow in a CFB riser. *AICHE J.* **1999**, *45*, 2503.
- (22) Goldschmidt, M. J. V.; Kuipers, J. A. M.; van Swaaij, W. P. M. Hydrodynamic modelling of dense gas-fluidized bed using the kinetic theory of granular flow. *Chem. Eng. Sci.* **2001**, *56*, 571.
- (23) Zhou, H.; Flamant, G.; Gauthier, D.; Lu, J. Lagrangian approach for simulating the gas-particle flow structure in a circulating fluidized bed riser. *Int. J. Multiphase Flow* **2002**, *28*, 1801.
- (24) Bokkers, G. A.; van Sint Annaland, M.; Kuipers, J. A. M. Mixing and segregation in a bidisperse gas-solid fluidised bed: a numerical and experimental study. *Powder Technol.* **2004**, *140*, 176.
- (25) Hoomans, B. P. B.; Kuipers, J. A. M.; Briels, W. J.; Van Swaaij, W. P. M. Discrete particle simulation of bubble and slug formation in a two-dimensional gas-fluidised bed: A hard-sphere approach. *Chem. Eng. Sci.* **1996**, *51*, 99.
- (26) Ergun, S. Fluid Flow through Packed Columns. *Chem. Eng. Progr.* **1952**, *48*, 89.
- (27) Wen, Y. C.; Yu, Y. H. Mechanics of Fluidization. *Chem. Eng. Progr. Symp. Ser.* **1966**, *62*, 100.
- (28) Gidaspow, D. *Multiphase Flow and Fluidization. Continuum and Kinetic Theory Description*; Academic Press: New York, 1994.
- (29) Vreman, B.; Geurts, B. J.; Deen, N. G.; Kuipers, J. A. M.; Kuerten, J. G. M. Two- and Four-Way Coupled Euler-Lagrangian Large-Eddy Simulation of Turbulent Particle-Laden Channel Flow. *Flow Turbul. Combust.* **2009**, *82*, 47–71.

Received for review October 9, 2008  
Revised manuscript received April 4, 2009

Accepted April 6, 2009

IE8015297